JACS
JOURNAL OF THE AMERICAN CHEMICAL SOCIETY
Article
pubs.acs.org/JACS

A Photoactive Porphyrin-Based Periodic Mesoporous Organosilica Thin Film

Yan Li,[†,§] Florian Auras,[†,§] Florian Löbermann,[†,§] Markus Döblinger,[†] Jörg Schuster,[†] Laurence Peter,[‡] Dirk Trauner,*[,†] and Thomas Bein*[,†]

[†]Department of Chemistry and Center for NanoScience (CeNS), University of Munich (LMU), Butenandtstrasse 5-13, 81377 Munich, Germany

[‡]Department of Chemistry, University of Bath, Clayerton Down, Bath BA2 7AY, United Kingdom

Supporting Information

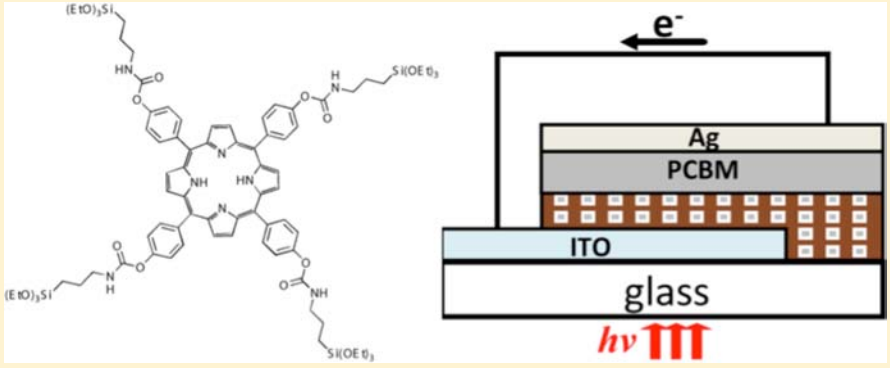

ABSTRACT: A novel optoelectroactive system based on an oriented periodic mesoporous organosilica (PMO) film has been developed. A tetra-substituted porphyrin silsesquioxane was designed as a precursor, and the porphyrin macrocycles were covalently incorporated into the organosilica framework without adding additional silica sources, using an evaporation-induced self-assembly process. The synthesized PMO film has a face-centered orthorhombic porous structure with a 15 nm pore diameter. This large pore size enables the inclusion of electron-conducting species such as [6,6]-phenyl C_{61} butyric acid methyl ester in the periodic mesopores. Optoelectronic measurements on the resulting interpenetrating donor−acceptor systems demonstrate the light-induced charge generation capability and hole-conducting property of the novel porphyrin-based PMO film, indicating the potential of PMO materials as a basis for optoelectroactive systems.

INTRODUCTION

Periodic mesoporous organosilica (PMO) materials have attracted considerable attention due to their structural and functional flexibility,[1−3] rendering them a versatile platform for fundamental research and potential applications in catalysis,[4−6] as adsorbents and functionalized scaffold materials,[7,8] and in optoelectronics.[9−12] These materials feature a unique combination of functional organic units and inorganic cross-linking parts within their periodically structured frameworks. In PMOs, each individual organic group is covalently bonded to two or more silicon atoms, such that the bridging organic unit is an integral part of the pore walls, rendering the mesopores easily accessible for guest molecules.

To date, numerous organic units from small aliphatic groups to larger aromatic groups have been successfully incorporated in the framework of PMO materials.[13−19] Recent developments of PMO materials were tailored toward the incorporation of photoactive and electroactive organic functionalities within their frameworks, aiming at their potential application in optoelectronic devices. It has been shown that the incorporation of building blocks with conjugated π-systems can produce fluorescent PMOs[11] or light harvesting systems, in which the energy absorbed by the PMO chromophore can be used for exciting a fluorescent dye that is located inside the pores.[12] Despite the insulating nature of the silica moiety, conductive PMOs can be realized if the packing of the organic building blocks can be controlled such that large π-stacked domains are formed.[20,21]

Porphyrins with their extended conjugated π-systems are capable of absorbing light throughout the visible range and are known to be effective donor materials in small molecule organic photovoltaics.[22] The large planar porphyrin units of a porphyrin-bridged silsesquioxane were reported to self-assemble into ordered superstructures, which consist of square arrays of porphyrin stacks.[23] However, porphyrin-containing PMO materials have been realized thus far only through the addition of a secondary silica source, which considerably dilutes the chromophores and compromises electronic interactions.[24,25]

Received: August 11, 2013
Published: November 5, 2013

   dx.doi.org/10.1021/ja4082028 | J. Am. Chem. Soc. 2013, 135, 18513−18519

Here we report that under optimized synthesis conditions a periodic mesoporous organosilica can be constructed solely from a porphyrin-based ethoxysilane precursor (Scheme 1)

Scheme 1. Chemical Structure of the Ethoxysilyl Precursor Containing a Porphyrin Macrocycle

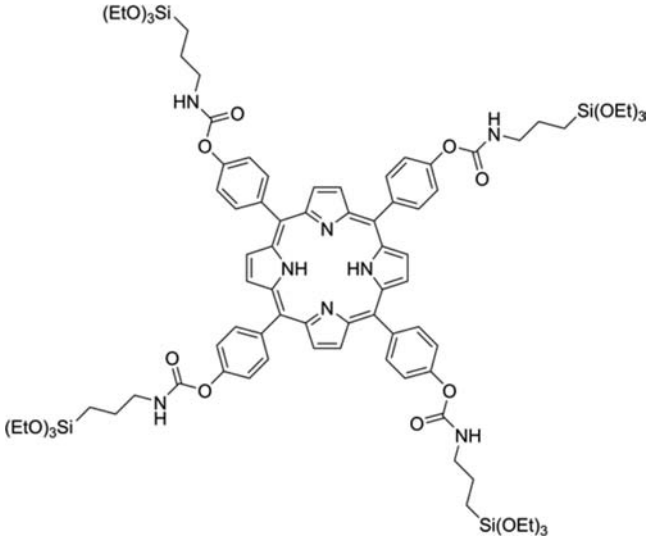

through an evaporation-induced self-assembly approach. When employing the triblock copolymer Pluronic F127 as a structure-directing agent, the resulting PMO films exhibit a face-centered orthorhombic structure with a pore size of 15 nm after template removal. This open-pore nanostructure facilitates the infiltration with an electron-acceptor phase and thereby the formation of a bicontinuous network. We observe light-induced charge transfer from the photoactive PMO to the acceptor and charge percolation through the network, leading to a photocurrent between charge carrier selective electrodes. Our results demonstrate the potential of such PMOs with high surface area as light harvesting scaffold for potential applications in photosensing, photocatalysis, and photoelectrochemistry.

RESULTS AND DISCUSSION

Mesostructured Porphyrin-Bridged PMO Films. The porphyrin-based PMO (Por-PMO) was synthesized by an evaporation-induced self-assembly (EISA) approach.[26] Mesostructured Por-PMO thin films were obtained by spin-coating an acidified solution containing the porphyrin ethoxysilyl precursor and the triblock copolymer Pluronic F127 in ethanol onto flat substrates, followed by slow evaporation of the solvent. We found that despite the considerable size of the precursor molecule, no addition of a second silica source was necessary. Figure 1 shows the small-angle X-ray scattering (SAXS) patterns of the as-deposited PMO film (a), after thermal annealing at 120 °C (b), and followed by solvent extraction (c). The as-prepared film exhibits a diffraction signal at 2θ = 0.86°, which indicates the formation of a periodic mesostructure with a *d*-spacing of 10.3 nm along the film normal. After thermal treatment and solvent extraction, the reflection positions are shifted to 0.92° and 1.33°, respectively, corresponding to *d*-spacings of 9.6 and 6.6 nm. The decreased *d*-spacings result from film shrinkage along the substrate normal, which is commonly observed for mesoporous thin films after template removal.[21,27−29]

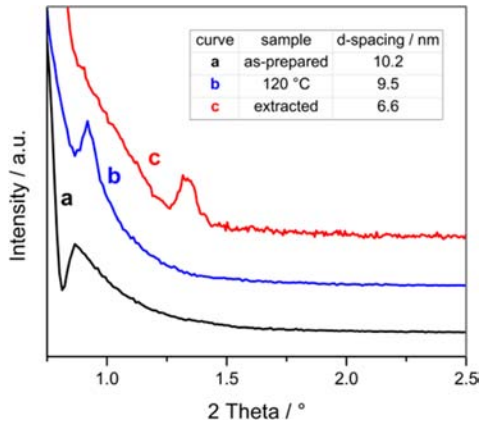

Figure 1. SAXS patterns of the Por-PMO films: (a) as prepared, (b) after thermal treatment at 120 °C for 5 h, (c) after extraction with ethanol. An offset has been added to the curves for clarity.

The 2D-grazing incidence small-angle X-ray scattering (GISAXS) pattern of the extracted Por-PMO film can be indexed to a face-centered orthorhombic unit cell (*Fmmm*) with the (010) plane parallel to the substrate (Figure 2). Transformations from an initial body-centered cubic micellar structure ($Im\bar{3}m$) to a *Fmmm* symmetry upon 1D shrinkage have been observed for mesoporous silica and carbon films that were synthesized using the same structure directing agent (Figure S1).[30−33] The GISAXS pattern of the Por-PMO resembles the patterns observed for these films of identical

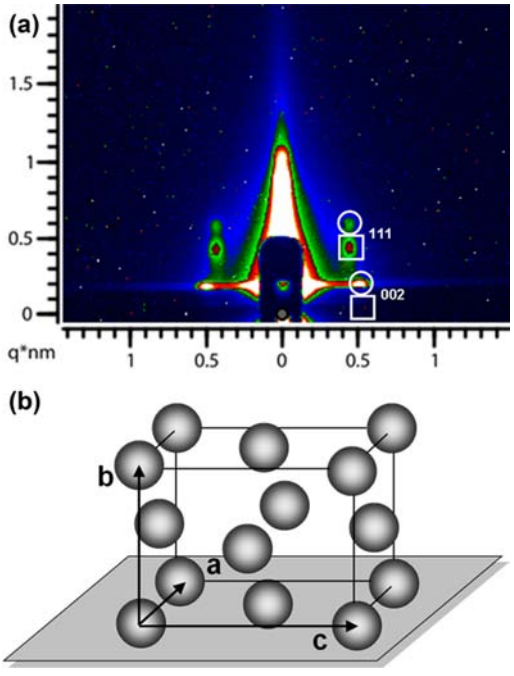

Figure 2. (a) 2D-GISAXS pattern (top) of the extracted Por-PMO film according to the face-centered orthorhombic symmetry (*Fmmm*) with the (010) plane parallel to the substrate. The reflections in the GISAXS pattern are doubled due to scattering of the primary beam before (squares) and after (circles) being reflected at the film−substrate interface. Hence, reflections on top of each other belong to the same set of lattice planes. The lower empty square denotes the position of the 002 reflection. As it is below the sample 'horizon', its intensity is fully absorbed by the sample. (b) Schematic illustration of the face-centered orthorhombic unit cell (bottom).

dx.doi.org/10.1021/ja4082028 | J. Am. Chem. Soc. 2013, 135, 18513−18519

symmetry and is similar to those observed for many mesoporous films after 1D shrinkage.[34,35] The lattice constants for the extracted Por-PMO film determined by SAXS and 2D-GISAXS are a = 17.5 nm, b = 13.2 nm, and c = 24.8 nm, if one defines the basis vectors **a** and **c** as parallel to the film and **b** along the film normal. The reflection observed in the 1D-SAXS pattern (Figure 1) thus can be indexed as 020.

Figure 3 shows a representative transmission electron micrograph of the Por-PMO film after solvent extraction. In the plan-view image, the periodic mesostructure of the Por-PMO film with domain sizes in the range of hundreds of nanometers can be observed. The presence of the ordered domains in the TEM image confirms that the mesostructure is preserved after removal of the surfactant template and that its molecular building blocks are cross-linked enough to render it stable against electron-beam damage during TEM characterization. The d-spacings determined from the TEM images and their Fourier transform are on average 9.6 and 13.3 nm, corresponding to the (200) and (002) sets of lattice planes. This observation fits well with the values expected for an *Fmmm* structure with the b-axis along the film normal, and the spacings are consistent with those obtained in SAXS measurements.

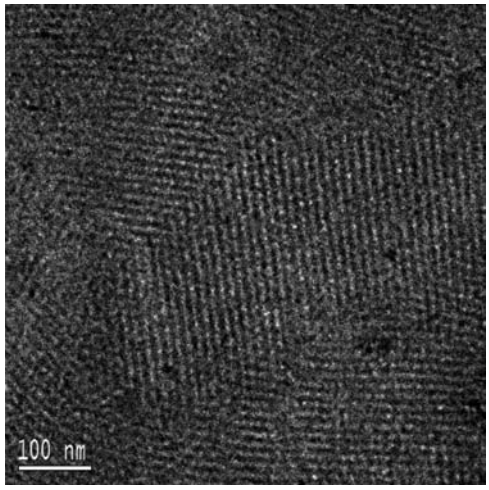

Figure 3. Plan-view TEM image of the extracted Por-PMO film. The presence of the ordered domains in the TEM image confirms the preservation of the mesostructure after removal of the surfactant template.

To investigate the porosity of the extracted Por-PMO material, nitrogen sorption isotherms of films removed from the substrate were recorded. Figure 4 shows the obtained isotherm with a typical type IV isotherm shape, which is commonly observed for mesoporous materials. The presence of the hysteresis loop indicates that the material features large, cage-like pores that are interconnected by pore openings of smaller diameter. Similar porosity properties with cage-like pores were also found for mesoporous carbon films of *Fmmm* symmetry, however, with much smaller pore sizes.[32] The Por-PMO was found to have a Brunauer–Emmett–Teller (BET) surface area of 364 $m^2\ g^{-1}$ and a pore volume of 0.57 $cm^3\ g^{-1}$. The NLDFT pore-size distribution calculated from the adsorption branch indicates that the extracted material has interconnected mesopores with a mean diameter of about 15 nm (inset of Figure 4). Such large pores enable the accommodation of sizable guest molecules into the 3D PMO mesostructure.

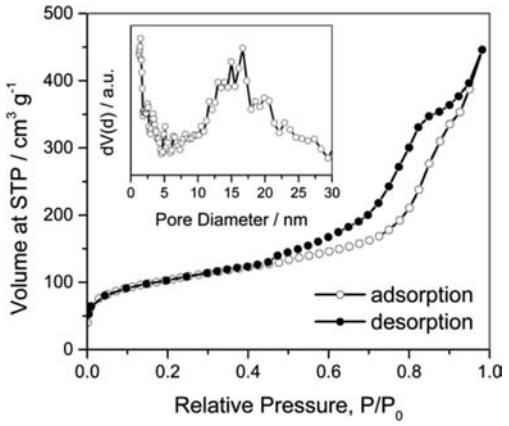

Figure 4. Nitrogen adsorption (○) and desorption (●) isotherms of the extracted Por-PMO material with an inset showing the pore size distribution calculated with the NLDFT method from the adsorption branch (○) using a SiO_2 kernel assuming cylindrical/spherical pore geometry for the sample. The increase of the pore size distribution below 5 nm is an artifact of the selected method.

The extracted Por-PMO material was furthermore investigated by solid-state NMR spectroscopy in order to get detailed information about the chemical environment of both ^{13}C and ^{29}Si nuclei in the PMO material. In the ^{13}C-MAS NMR spectrum (Figure 5a), the detected chemical shifts in the range of 100–160 ppm are assigned to the carbon atoms in the aromatic ring of the porphyrin moiety.[36–39] The signals at 7.8 ppm ($SiCH_2$), 23.2 ppm ($SiCH_2CH_2$), 42.1 ppm (CH_2NH), and 155.4 ppm (C═O) can be assigned to the carbon atoms in the propyl isocyanate moiety.[40–44] The ^{13}C NMR spectrum proves that the porphyrin-based organic bridges in the precursor are robust enough to survive the synthesis conditions. In the solid-state ^{29}Si MAS NMR spectrum (Figure 5b), chemical shifts of T^1 [$CSi(OSi)(OH)_2$], T^2 [$CSi(OSi)_2(OH)$], and T^3 [$CSi(OSi)_3$] sites were observed at −46.5, −57.8, and −65.7 ppm, respectively.[45,46] No signals were observed in the range of −100 to −125 ppm, which would be representative of Q^n sites [Q^n = $Si(OSi)_n(OH)_{4-n}$], confirming that the Si–C bonds are stable and completely retained in the final mesoporous framework.[47–49]

Optical Properties. The UV–vis spectra of a dilute solution containing the porphyrin-bridged precursor as well as that of the extracted Por-PMO film are shown in Figure 6. For the dilute precursor solution, a strong Soret band is observed at 417 nm. Additionally, four bands are observed at 514, 551, 593, and 649 nm, which can be assigned to the Q-band signals that are typical for nonaggregated, free-base porphyrin units.[39,50,51] The absorption bands of the extracted Por-PMO film have similar shape but are red-shifted compared to the spectrum of the precursor solution. Similar red-shifts have been observed in other systems with assembled porphyrin macrocycles and are believed to result from densely packed molecular aggregates that allow electronic coupling and energy transfer among the porphyrin building blocks.[23,52,53]

Optoelectronic Properties. In order to investigate the photoactive and electronic properties of the Por-PMO system we prepared films of about 100 nm thickness on indium tin oxide (ITO) coated glass substrates.

For an optoelectronic characterization of the Por-PMO film we chose an aqueous electrolyte containing 0.1 M KNO_3 and 1 mM H_2O_2 due to its low redox potential, which facilitates fast

dx.doi.org/10.1021/ja4082028 | J. Am. Chem. Soc. 2013, 135, 18513–18519

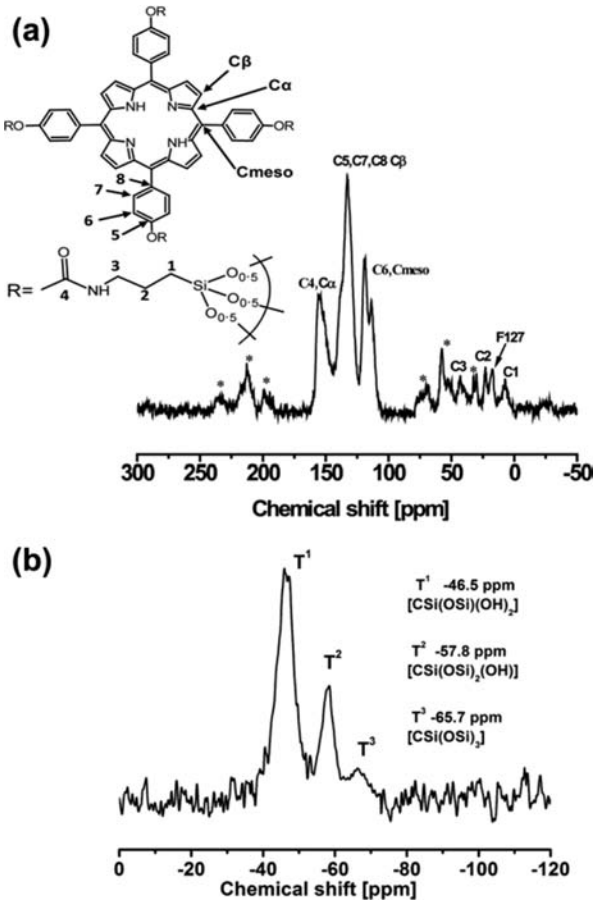

Figure 5. (a) ^{13}C CP-MAS NMR and (b) ^{29}Si CP-MAS NMR spectra of the extracted Por-PMO material with the corresponding assignments of the different resonances. Signals with asterisk * are spinning side bands.

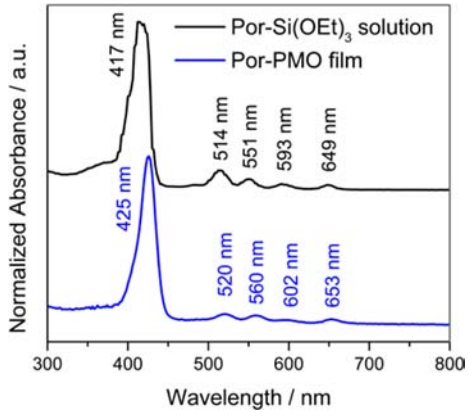

Figure 6. UV–vis absorption spectra of a dilute solution containing 10^{-5} M porphyrin ethoxysilyl precursor in THF (black) and the extracted Por-PMO film (blue). For clarity, an offset is added to the black curve.

charge transfer. Moreover, the electrolyte features good transparency over the entire visible spectral range. The Por-PMO film was connected as working electrode, and a Pt wire was used as counter electrode (Figure 7a). The time-resolved photocurrent response and the spectrally resolved photoresponse were investigated.

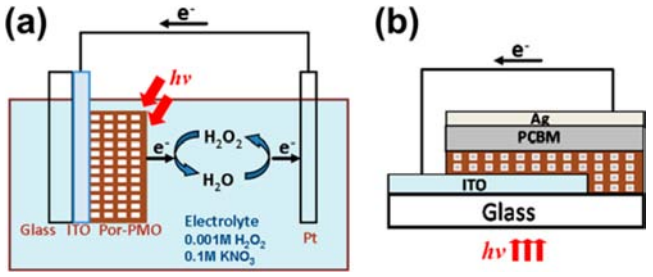

Figure 7. Illustration of (a) the experimental setup for optoelectrochemical experiments in a redox electrolyte and (b) the configuration of the solid-state devices based on a PCBM-infiltrated Por-PMO film.

Current transients were recorded at different intensities of simulated solar light with illumination from the film side (Figure 8a). A current pulse is generated upon illumination and quickly decays to a lower steady-state current. A pulse of similar amplitude but opposite sign is observed when switching the light off. These anodic and cathodic current spikes are well-known for films of organic semiconductors in electrolytes and

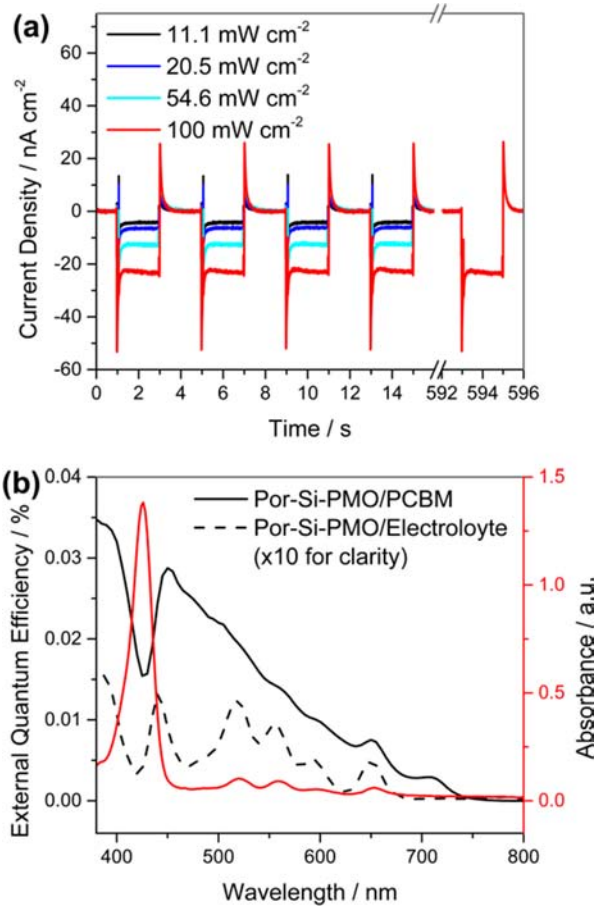

Figure 8. (a) Time-resolved photocurrent response of the extracted Por-PMO film deposited on ITO in an aqueous electrolyte containing 0.1 M KNO_3 and 1 mM H_2O_2 (active area is 1 cm^2). The experiment was carried out using simulated AM1.5G solar light of different light intensities. (b) EQE of the Por-PMO:PCBM solid-state device (solid line) and of a Por-PMO film in the electrolyte (dashed line) and UV–vis spectrum of a Por-PMO film (red line). The spectrum measured in the electrolyte was multiplied by 10 for clarity.

dx.doi.org/10.1021/ja4082028 | J. Am. Chem. Soc. 2013, 135, 18513–18519

are believed to originate from charging and discharging of surface states.[54−56] The sign of the photocurrent identifies the Por-PMO film as a p-type semiconductor, indicating that electron−hole pairs are generated upon illumination and that the electrons are transferred to the electrolyte, whereas the holes are transported within the Por-PMO film. The current output under full sun illumination remained unchanged during 150 illumination/dark cycles. We furthermore investigated the current generation capabilities of the Por-PMO at different light intensities and found a nonlinear dependence of the steady-state current on the illumination density (Figure S4). This behavior is known from transport-limited solar cells. As the concentration of photogenerated holes inside the PMO film is increased at high light intensities, the probability of non-geminate recombination is increased as well, resulting in lower charge carrier collection efficiency.

In addition to the time-resolved photocurrent we recorded the spectrally resolved photocurrent at short circuit (Figure 8b, dashed line). Above 500 nm, the spectrum of the external quantum efficiency (EQE), which is the ratio of collected electrons to incident photons, closely resembles the absorbance spectrum of the Por-PMO film. However, around 420 nm, where the porphyrin has its strongest absorption, we observe a 'dip' in the EQE spectrum. Assuming similar recombination lifetimes throughout the film, the collection efficiency for photogenerated holes will depend on the distance to the electrode, thus rendering the volume close to the ITO interface most effective for current production. The light available in this region, however, differs in its spectral distribution from the incident light due to absorption on its way through the PMO film (Figure S5a). The shape of the EQE spectrum will consequently be governed by the light that is absorbed in this region. We indeed find that the EQE spectrum of the Por-PMO film closely resembles the simulated spectrum of photons absorbed close to the electrode interface (Figure S5b), thereby illustrating the nonuniform current collection due to recombination losses in this material.

We also combined the hole-transporting Por-PMO films with an electron acceptor to form a 3D solid-state heterojunction. Soaking the extracted mesoporous films in a solution of [6,6]-phenyl C_{61} butyric acid methyl ester (PCBM), followed by spin-coating leads to infiltration of the electron-transporting species into the mesopores (confirmed by N_2 sorption, Figure S2) and the formation of an additional PCBM overlayer of about 20 nm. This overlayer is desired in order to form an electron-selective contact with the Ag back electrode and to avoid short-circuiting the device through direct contact of the Ag with the hole-transporting PMO (configuration of the device illustrated in Figure 7b, SEM image in Figure S3).

The EQE spectrum of the device follows the absorbance trend of the Por-PMO film except in the region around 420 nm (Figure 8b, solid line). Compared to the measurements in an electrolyte the photocurrent response in the blue and UV part of the spectrum is much higher, which we attribute to a contribution of the PCBM. The observed photocurrent appears to be a superposition of excitons generated in the Por-PMO followed by electron injection into the PCBM, and excitons generated upon light absorption by the PCBM followed by hole injection into the Por-PMO. As already observed for the liquid electrolyte sample, the photocurrent generated at the strongest absorption peak of the porphyrin framework is in fact lower than at neighboring wavelengths. At around 420 nm, since the illumination is through the ITO substrate in the case of the solid-state Por-PMO:PCBM device, most excitons are created close to the ITO front contact. In this case the charge carrier collection efficiency seems to be highest for a region that is close to the PMO film surface, possibly due to the formation of a PCBM gradient upon infiltration. Similar to the case discussed above for the PMO film in the electrolyte, the light intensity in the most active region of the device is altered by the strong absorption of the Soret band, resulting in a 'dip' in the EQE spectrum.

CONCLUSION

A novel periodic mesoporous organosilica film material was successfully synthesized by polycondensation of a specially designed porphyrin-containing organosilane precursor in the presence of a surfactant template. The resulting PMO film possesses a 3D orthorhombic mesostructure with a large pore size of 15 nm. The PMO film exhibits broad-band light absorption due to the incorporated porphyrin moieties. We have demonstrated the possibility of forming a periodic 3D heterojunction by infiltrating the PMO film with an electron-acceptor phase. Moreover, we were able to prove light-induced charge transfer from the porphyrin PMO to the acceptor and charge percolation through the porphyrin PMO, which results in a photocurrent output upon simulated solar illumination. Our results demonstrate the potential of chromophore-containing PMOs with high surface area as periodic light-harvesting scaffolds, which render them structurally well-defined model systems for studying photoactive building blocks.

EXPERIMENTAL SECTION

Preparation of Por-PMO Films. 0.075 g (0.045 mmol) porphyrin-containing precursor (Figure 1, synthetic procedures in the Supporting Information) and 0.075 g (0.006 mmol) Pluronic F127 were first dissolved in 2.4 mL ethanol. Next, 0.08 mL of 0.1 M HCl (8.0×10^{-3} mmol) was added, and the resulting solution was stirred at room temperature for 4 h. Finally, the aged sol was spin-coated on glass slides (2×2 cm^2) at 3000 rpm for 30 s. The obtained films were dried in air at room temperature overnight. In order to fully condense the silica units and remove the surfactant, the films were heated in flowing N_2 with a ramp of 1 °C min^{-1} to 120 °C and kept at this temperature for 5 h and finally refluxed in absolute ethanol for 2 h.

Structural Characterization. SAXS was carried out using a Bruker D8 Discover with Ni-filtered CuK_α radiation (0.154 nm) and a position-sensitive detector (LynxEye). For 2D-GISAXS characterization, a SAXSess system by Anton Paar (CuK_α radiation, sample−detector distance 306.7 mm) with a CCD detector (PI-SCX:4300, Roper Scientific) was used. The samples were measured for 10 h with a tilt angle of 0.27° with respect to the primary beam. TEM was performed using a FEI Titan 80-300 instrument equipped with a field emission gun operated at 300 kV. Nitrogen sorption measurements were carried out at −196 °C using an Autosorb-1 (Quantachrome Instruments). Samples were degassed at 150 °C for 12 h in vacuum prior to measurement. For the sorption experiments thicker films were synthesized by drop-casting the same solution as described above on flat glass substrates. After thermal treatment, these thick films were scratched off from the glass slides and refluxed in absolute ethanol to remove the surfactant template. The BET surface area was calculated using experimental points at a relative pressure range of $p/p_0 = 0.05-0.20$. The total pore volume was calculated from the N_2 amount adsorbed at the highest p/p_0 ($p/p_0 = 0.98$). NLDFT pore size distributions were calculated from the adsorption branch using a SiO_2 kernel and assuming a cylindrical/spherical pore geometry. Solid-state ^{13}C and ^{29}Si NMR experiments were performed on a Bruker Avance-III 500 spectrometer (11.7 T) operating at frequencies of 125.8 MHz for ^{13}C and 99.4 MHz for ^{29}Si. $^{13}C(^1H)$ CP-MAS spectra were

dx.doi.org/10.1021/ja4082028 | J. Am. Chem. Soc. 2013, 135, 18513−18519

acquired using a 90° pulse length of 2.5 μs (3.7 dB) with cross-polarization contact time of 5 ms and a recycle delay of 2 s. $^{29}Si(^{1}H)$ CP-MAS experiments were conducted using a 90° pulse length of 2.5 μs (3.7 dB) with cross-polarization contact time of 5 ms and a recycle delay of 2 s.

Photoelectrochemical Characterization. Por-PMO films for photoelectrochemical characterization were synthesized on indium tin oxide coated glass (VisionTek, 150 nm ITO, 12−15 ohms/sq).

UV−vis measurements were performed on a Hitachi U3501 spectrophotometer equipped with an integrating sphere. Absorbance spectra were recorded in transmission geometry with plain ITO as reference.

For the measurements in an electrolyte, the ITO substrates were cut into pieces of 1 × 1.5 cm^2. A 5 mm wide contact area on one side of the substrate was masked during the deposition of the PMO film, resulting in an active area of 1 cm^2. After extraction of the template the blank part of the ITO was contacted with a copper wire using silver paste, and then this contact area was sealed with poly(dimethylsiloxane) in order to avoid direct contact between the ITO and the electrolyte. Photoelectrochemical measurements were performed with the Por-PMO film as working electrode and a platinum wire as counter electrode in an aqueous electrolyte containing 0.1 M KNO_3 and 1 mM H_2O_2.

Solid-state devices were fabricated on patterned ITO substrates. After deposition of the PMO layer and subsequent extraction of the template, the films (1.5 × 1.5 cm^2) were immersed overnight into a solution of PCBM (3 mg mL^{-1} in chlorobenzene) to enhance the infiltration of the PCBM into the mesopores. The films were then taken from this solution and immediately spin-coated at 1000 rpm for 60 s, which resulted in a thin and homogeneous layer of PCBM on top of the PMO film. Finally, 70 nm thick silver contacts were sputter deposited through a shadow mask, yielding an active area of 16 mm^2. The samples were illuminated through a 12 mm^2 mask and measured in air.

For recording current transients the samples were illuminated with white light from an AM1.5G solar simulator (Solar Light Model 16S) at 100 mW cm^{-2}, which was modulated by a shutter. Illumination was carried out from the film side in case of the measurements in an electrolyte and through the ITO substrate in case of the solid-state devices. Lower light intensities were realized with a set of calibrated reflective neutral density filters. The signal was recorded using a low noise preamplifier (Femto DLPCA-200) and an oscilloscope (Tektronix DPO2012).

EQE measurements were performed at short circuit. Monochromatic light was obtained from a 150 W xenon lamp in combination with a monochromator and order-sorting filters. The slits were adjusted such that the fwhm was 5 nm at a light intensity of approximately 2 mW cm^{-2}. All light intensities were calibrated with a Fraunhofer ISE certified silicon reference cell equipped with a KG5 filter. The monochromatic light was modulated using an optical chopper at a frequency of 4 Hz for measurements in an electrolyte and 12 Hz in case of the solid-state devices. The signal was detected via a low-noise preamplifier (Femto DLPCA-200) and a lock-in amplifier (Signal Recovery 7265). The modulation frequency was chosen slow enough such that the current response of the sample was square-like.

■ ASSOCIATED CONTENT

Supporting Information

Synthetic procedure of the porphyrin-containing ethoxysilane precursor, the sorption isotherm of Por-PMO with PCBM infiltrated into the mesopores, and additional information on the optoelectronic characterization. This material is available free of charge via the Internet at http://pubs.acs.org.

■ AUTHOR INFORMATION

Corresponding Authors

dirk.trauner@cup.uni-muenchen.de
tbein@lmu.de

Author Contributions

[§]These authors contributed equally.

Notes

The authors declare no competing financial interest.

■ ACKNOWLEDGMENTS

We thank the Deutsche Forschungsgemeinschaft through the SFB 486, the LMUexcellent program, the Nanosystems Initiative Munich (NIM cluster), the SolTech network (Bavaria), and the China Scholarship Council (CSC) for supporting this work.

■ REFERENCES

(1) Asefa, T.; MacLachlan, M. J.; Coombs, N.; Ozin, G. A. *Nature* **1999**, *402*, 867.
(2) Inagaki, S.; Guan, S.; Fukushima, Y.; Ohsuna, T.; Terasaki, O. *J. Am. Chem. Soc.* **1999**, *121*, 9611.
(3) Melde, B. J.; Holland, B. T.; Blanford, C. F.; Stein, A. *Chem. Mater.* **1999**, *11*, 3302.
(4) Yang, Q.; Liu, J.; Zhang, L.; Can, L. *J. Mater. Chem.* **2009**, *19*, 1945.
(5) Kuschel, A.; Polarz, S. *J. Am. Chem. Soc.* **2010**, *132*, 6558.
(6) Jeong, E.-Y.; Ansari, M. B.; Park, S.-E. *ACS Catal.* **2011**, *1*, 855.
(7) Li, C.; Liu, J.; Shi, X.; Yang, J.; Yang, Q. *J. Phys. Chem. C* **2007**, *111*, 10948.
(8) Park, M.; Park, S. S.; Selvaraj, M.; Zhao, D.; Ha, C.-S. *Microporous Mesoporous Mater.* **2009**, *124*, 76.
(9) Hernandez, R.; Franville, A.-C.; Minoofar, P.; Dunn, B.; Zink, J. I. *J. Am. Chem. Soc.* **2001**, *123*, 1248.
(10) Minoofar, P. N.; Hernandez, R.; Chia, S.; Dunn, B.; Zink, J. I.; Franville, A.-C. *J. Am. Chem. Soc.* **2002**, *124*, 14388.
(11) Mizoshita, N.; Goto, Y.; Tani, T.; Inagaki, S. *Adv. Funct. Mater.* **2008**, *18*, 3699.
(12) Inagaki, S.; Ohtani, O.; Goto, Y.; Okamoto, K.; Ikai, M.; Yamanaka, K.-i.; Tani, T.; Okada, T. *Angew. Chem., Int. Ed.* **2009**, *48*, 4042.
(13) Sayari, A.; Wang, W. *J. Am. Chem. Soc.* **2005**, *127*, 12194.
(14) Morell, J.; Güngerich, M.; Wolter, G.; Jiao, J.; Hunger, M.; Klar, P. J.; Fröba, M. *J. Mater. Chem.* **2006**, *16*, 2809.
(15) Takeda, H.; Goto, Y.; Maegawa, Y.; Ohsuna, T.; Tani, T.; Matsumoto, K.; Shimada, T.; Inagaki, S. *Chem. Commun.* **2009**, *45*, 6032.
(16) Vercaemst, C.; de Jongh, P. E.; Meeldijk, J. D.; Goderis, B.; Verpoort, F.; Van Der Voort, P. *Chem. Commun.* **2009**, *45*, 4052.
(17) Kapoor, M. P.; Yang, Q.; Inagaki, S. *J. Am. Chem. Soc.* **2002**, *124*, 15176.
(18) Mizoshita, N.; Tani, T.; Inagaki, S. *Chem. Soc. Rev.* **2011**, *40*, 789.
(19) Cornelius, M.; Hoffmann, F.; Fröba, M. *Chem. Mater.* **2005**, *17*, 6674.
(20) Mizoshita, N.; Tani, T.; Inagaki, S. *Adv. Funct. Mater.* **2011**, *21*, 3291.
(21) Mizoshita, N.; Ikai, M.; Tani, T.; Inagaki, S. *J. Am. Chem. Soc.* **2009**, *131*, 14225.
(22) Martínez-Díaz, M. V.; de la Torre, G.; Torres, T. *Chem. Commun.* **2010**, *46*, 7090.
(23) Peng, H.; Lu, Y. *Adv. Mater.* **2008**, *20*, 797.
(24) Jeong, E.-Y.; Burri, A.; Lee, S.-Y.; Park, S.-E. *J. Mater. Chem.* **2010**, *20*, 10869.
(25) Johnson-White, B.; Zeinali, M.; Shaffer, K. M.; Patterson, C. H., Jr.; Charles, P. T.; Markowitz, M. A. *Biosens. Bioelectron.* **2007**, *22*, 1154.
(26) Brinker, C. J.; Lu, Y.; Sellinger, A.; Fan, H. *Adv. Mater.* **1999**, *11*, 579.
(27) Miyata, H.; Kuroda, K. *Chem. Mater.* **2000**, *12*, 49.
(28) Schuster, J.; Köhn, R.; Keilbach, A.; Döblinger, M.; Amenitsch, H.; Bein, T. *Chem. Mater.* **2009**, *21*, 5754.

(29) Ortel, E.; Reier, T.; Strasser, P.; Kraehnert, R. *Chem. Mater.* **2011**, *23*, 3201.
(30) Falcaro, P.; Grosso, D.; Amenitsch, H.; Innocenzi, P. *J. Phys. Chem. B* **2004**, *108*, 10942.
(31) Urade, V. N.; Hillhouse, H. W. *J. Phys. Chem. B* **2005**, *109*, 10538.
(32) Tanaka, S.; Katayama, Y.; Tate, M. P.; Hillhouse, H. W.; Miyake, Y. *J. Mater. Chem.* **2007**, *17*, 3639.
(33) Schuster, J.; Köhn, R.; Döblinger, M.; Keilbach, A.; Amenitsch, H.; Bein, T. *J. Am. Chem. Soc.* **2012**, *134*, 11136.
(34) Tate, M. P.; Urade, V. N.; Kowalski, J. D.; Wei, T.-c.; Hamilton, B. D.; Eggiman, B. W.; Hillhouse, H. W. *J. Phys. Chem. B* **2006**, *110*, 9882.
(35) Song, L.; Feng, D.; Campbell, C. G.; Gu, D.; Forster, A. M.; Yager, K. G.; Fredin, N.; Lee, H.-J.; Jones, R. L.; Zhao, D.; Vogt, B. D. *J. Mater. Chem.* **2010**, *20*, 1691.
(36) Frydman, L.; Olivieri, A. C.; Díaz, L. E.; Valasinas, A.; Frydman, B. *J. Am. Chem. Soc.* **1988**, *110*, 5651.
(37) Tung, J.-Y.; Chen, J.-H.; Liao, F.-L.; Wang, S.-L.; Hwang, L.-P. *Inorg. Chem.* **1998**, *37*, 6104.
(38) Feng, X.; Chen, L.; Dong, Y.; Jiang, D. *Chem. Commun.* **2011**, *47*, 1979.
(39) Wan, S.; Gándara, F.; Asano, A.; Furukawa, H.; Saeki, A.; Dey, S. K.; Liao, L.; Ambrogio, M. W.; Botros, Y. Y.; Duan, X.; Seki, S.; Stoddart, J. F.; Yaghi, O. M. *Chem. Mater.* **2011**, *23*, 4094.
(40) Lee, J.-S.; Ryu, S.-W. *Macromolecules* **1999**, *32*, 2085.
(41) Bass, J., D.; Katz, , A. *Chem. Mater.* **2003**, *15*, 2757.
(42) Mel'nik, I. V.; Lyashenko, O. V.; Zub, Y. L.; Chuiko, A. A.; Cauzzi, D.; Predieri, G. *Russ. J. Gen. Chem.* **2004**, *74*, 1782.
(43) Yan, B.; Ma, D.-J. *J. Solid State Chem.* **2006**, *179*, 2059.
(44) Francis, B.; Raj, D. B. A.; Reddy, M. L. P. *Dalton Trans.* **2010**, *39*, 8084.
(45) Takafuji, M.; Azuma, N.; Miyamoto, K.; Maeda, S.; Ihara, H. *Langmuir* **2009**, *25*, 8428.
(46) Radi, B.; Wellard, R. M.; George, G. A. *Macromolecules* **2010**, *43*, 9957.
(47) Keilbach, A.; Döblinger, M.; Köhn, R.; Amenitsch, H.; Bein, T. *Chem.—Eur. J.* **2009**, *15*, 6645.
(48) Wahab, M. A.; He, C. *Langmuir* **2009**, *25*, 832.
(49) Li, Y.; Keilbach, A.; Kienle, M.; Goto, Y.; Inagaki, S.; Knochel, P.; Bein, T. *J. Mater. Chem.* **2011**, *21*, 17338.
(50) García-Sánchez, M. A.; Campero, A. *J. Non-Cryst. Solids* **2001**, *296*, 50.
(51) García-Sánchez, M. A.; Campero, A. *J. Non-Cryst. Solids* **2004**, *333*, 226.
(52) Maiti, N. C.; Mazumdar, S.; Periasamy, N. *J. Phys. Chem. B* **1998**, *102*, 1528.
(53) De la Luz, V.; García-Sánchez, M. A.; Campero, A. *J. Non-Cryst. Solids* **2007**, *353*, 2143.
(54) Oekermann, T.; Schlettwein, D.; Jaeger, N. I. *J. Electroanal. Chem.* **1999**, *462*, 222.
(55) Schlettwein, D.; Karmann, E.; Oekermann, T.; Yanagi, H. *Electrochim. Acta* **2000**, *45*, 4697.
(56) Oekermann, T.; Schlettwein, D.; Jaeger, N. I. *J. Phys. Chem. B* **2001**, *105*, 9524.